A Comprehensive Analysis of a Novel Real-time Adaptive Assist-as-needed Controller for Robot-assisted Rehabilitation for Stroke Patients

Ana Paula Arantes (anapbba@gmail.com)
Institute of Biomedical Engineering, University of New Brunswick
Nadja Bressan
University of Prince Edward Island Faculty of Sustainable Engineering Design
Chris McGibbon
University of New Brunswick Institute of Biomedical Engineering

Research

Keywords: Rehabilitation therapy, electromyographical-based adaptive assist-as-needed (aAAN), speed and electrophysiological metrics (EMG and EEG)

Posted Date: January 6th, 2021

DOI: https://doi.org/10.21203/rs.3.rs-139605/v1

A comprehensive analysis of a novel real-time adaptive assist-as-needed controller for robot-assisted rehabilitation for stroke patients.

[1]Ana Paula B. B. Arantes, [2]Nadja Bressan, and [1,3]Chris McGibbon

1. Institute of Biomedical Engineering, University of New Brunswick; 2. Dept. Sustainable Engineering Design, University of Prince Edward Island; 3. Faculty of Kinesiology, University of New Brunswick

A comprehensive analysis of a novel real-time adaptive assist-as-needed controller for robot-assisted rehabilitation for stroke patients.

[1]Ana Paula B. B. Arantes, [2]Nadja Bressan, and [1,3]Chris McGibbon

Abstract

Background: Rehabilitation therapy plays an essential role in assisting stroke patients in regaining function. For this reason, many studies have been conducted to optimize rehabilitation interventions to improve effectiveness and efficiency. In this context, robotic devices for rehabilitation and assistance can be effective. Several studies have demonstrated that using a robot as a therapy tool can significantly reduce motor impairment. However, the slacking behavior, in which the patient lets the robot guide their movements even when they are capable of doing so by themselves, has been identified as a major barrier to reaching the full potential of robot-assist rehabilitation. This paper developed a novel electromyographical-based adaptive assist-as-needed (aAAN) controller aiming to avoid this slacking behavior. **Methods**: Five stroke patients were recruited to test the controller. Motor impairment status was documented with the Fugl-Meyer (FMA) assessment. In this experiment, horizontal arms tasks were conducted with the robot off and on to assess the subject's performance in both scenarios. Velocity, time, and position were quantified as performance parameters during the training. Arm and shoulder EMG and electroencephalography (EEG) were used to assess the performance of the controller. **Results**: The cross-sectional results showed strong second-order relationships between Fugl-Meyer score and outcome measures, where performance metrics (path length and accuracy) were sensitive to change in participants with lower functional status. In comparison, speed and electrophysiological metrics (EMG and EEG) were more sensitive to change in participants with higher functional status. EEG signal amplitude increased when the robot suggested that the robot was inducing a challenge during the training tasks. **Conclusion**: The preliminary results were very promising; slacking was avoided for all participants during training with the aAAN controller.

Introduction

Stroke is a leading cause of adult long-term serious disability and the second cause of mortality worldwide (1). According to the Public Health Agency of Canada and the Heart and Stroke Foundation, approximately 741,800 adults (365,000 men and 376,800 women) aged over 20 years old live with the effects of a stroke (2012/13). Stroke damages the brain, and 80% of people who suffered a stroke have hemiparesis, which is an impaired motor control on the affected side (2). Most survivors of hemispheric stroke present limited movement of the contralesional upper extremity.

Robots for assessment, treatment, and assistance of people with impaired motor control have shown some promise in improving motor recovery post-stroke. Although not readily available in clinics, the use of this technology in the rehabilitation field is widely thought to be potentially beneficial (3-13).

Most of the advanced work in the robot-assisted therapies field has been done in recent decades. Several studies have shown how the strategy of control used in robot-assisted rehabilitation can significantly and positively impact the rehabilitation process's effectiveness and efficiency (3,4,6,8-12). However, these studies indicate that most of the strategies used in robot-assisted therapies have drawbacks such as being susceptible to a “slacking” behavior where the subjects let the robot drive the movements without performing sufficient physical effort to benefit from the training. Moreover, an overall analysis of the subject’s progress, including muscle and brain activity, is crucial to understand motor learning and neuroplasticity process in stroke patients.

Prior studies also do not utilize an online adaptation of the control system based on physiological measurements that can appropriately scale assistance or resistance according to user performance and progression. To date, no study has done a comprehensive analysis of cortical activity when applied to a robotic-assisted training program for improving motor recovery in post-stroke patients (3,9,11,12).

The present study aimed to develop and validate a novel adaptive AAN (aAAN) algorithm for upper-extremity robot-assisted therapy for stroke. This new algorithm's control system integrates sEMG and a haptic system to provide a patient-cooperative non-slacking robotic-assisted therapy to facilitate and accelerate upper extremity motor function recovery. Changes in performance metrics, muscle, and brain activity between the baseline and training sessions were

examined for each subject. Relationships of these responses to participants' functional status using the Fugl-Meyer (FMA) clinical assessment were explored to quantify the robot training system's sensitivity. This enabled us to validate how outcomes measures would be expected to change with improvement in functional status. Specifically, we address the following research questions: Does overall mean EMG entropy amplitude increase when training with the aAAN algorithm?; Does overall mean EEG power density increase when training with the aAAN algorithm?; Are performance metrics that are assessed during training sensitive to functional status via the FMA score?; Is mean EMG entropy amplitude assessed during training sensitive to functional status via the FMA score?; Is mean EEG power density assessed during training sensitive to functional status via the FMA score?

Methods

To develop the robot-assisted training with an adaptive assist-as-needed system, the following essential requirements were prescribed. First, the robot shall provide enough force to allow the user to complete the task and motivate them but do so minimally to avoid the slacking effect. Second, the system shall adapt to the user's needs by, for example, reducing the assistance and increasing the challenge as the user's performance improves. Third, the training should be non-monotonic in order to be more engaging. These elements are expected to encourage voluntary control during training, known to promote motor plasticity in the brain (19,20). Finally, multiple sensors should be used for measuring movement performance and muscle and brain activity during the training to capture outcomes relevant to motor recovery.

Instrumentation

The system was implemented using a PHANTOM 3.0 device from SensAble technologies, with open-source software that allows the user to interact with it in a broad range of applications. This device is mostly used for rehabilitation, the development of games, and entertainment (15). It can provide low-level control, support the visualization of 3D objects, and can generate force effects. The PHANTOM device is a high-precision instrument connected to the computer through

a serial connection and provides a large workspace and high forces with high fidelity and low friction. Information such as velocity, force, and position can be provided from this device.

This study's EMG system was the Trigno™ Wireless EMG (Delsys, Inc., Natick, Massachusetts). This system has 16 active wireless sensors, with an EMG signal range of ±5V and a significant 909V/V ±5% gain. It also has an active analog bandpass filter between 10–500Hz, 160dB/Dec. The electrode placement and target group muscle that was used in this control system were the biceps (BI), triceps (TI), pectorallis major (PM), anterior deltoid (AD), middle deltoid (MD), and posterior deltoid (PD). The electrode placement followed the SENIAM guidelines.

The EEG, from Artinis company (Artinis Medical Systems, Einsteinweg, The Netherlands) has 128 channels EEG for full head coverage. Although the EEG signal is a spatially imprecise recording technique due to volume conduction (activation several centimeters away is recorded by electrodes), it is a very useful technique as it records at a very high sample rate of up to several tens of Kilohertz.

Control algorithm

The information acquired in real-time from the PHANTOM and EMG systems was used to control the robot-assisted system. Prior studies have utilized muscle activity or user's performance and velocity data to develop strategies of control with different levels of assistance. To our best knowledge, no studies have validated this approach or integrated the capability of challenging the users to keep them engaged. Past research shows this is a requirement to promote motor plasticity and a faster recovery (5-7, 10,11,17).

For the novel patient-cooperative non-slacking system, the system's initial trigger is regulated based on the EMG signal. The EMG control part of the system was similar to the approach described in Zhang et al. (27), where the sample entropy was computed for the EMG signal in order to detect the muscle activity onset. The entropy of an EMG signal represents the complexity and randomness of the signal. This measurement takes advantage of this dynamic system's nonlinear properties to distinguish voluntary surface EMG signals from spurious background spikes. The calculation of the entropy of the EMG signal starts by embedding the scalar time series $\{x_1, x_2, \dots, x_{n,}\}$ in a delay m-dimensional space as the following:

$$x(p) = [x(p+k)]_{k=0}^{m-1}, p = 1, 2, \ldots, n-m+1$$

Then, the sample entropy is calculated as the following:

$$SampEn(x, m, r) = -ln(\frac{A^m(r)}{B^m(r)})$$

where B(r) is the probability of two sequences matching for m points, which is calculated by counting the average number of vector pairs where the distance is lower than the tolerance r and where A(r) is an embedding dimension of m+1. Once this is done, the EMG trigger threshold is determined based on the signal resulting from this process.

The EMG signal of three muscles was constantly analyzed. The velocity was also constantly acquired as soon as the EMG trigger threshold first trigged the system. The robot only assisted the patient if the system has been triggered and the muscle is maintained activated, but the insufficient motion is detected to achieve the target. Figure 1 illustrates how this method works.

Figure 1: Patient-cooperative non-slacking system

The system adapts to the subject's progress based on their sEMG signal, the velocity, and force data he or she can generate throughout the training sessions. The EMG threshold value gradually increases, and some resistance force is gradually added to the system once the driving muscle can generate stronger EMG signals. The performance of the subject improves. The initial threshold (buffer) was calculated based on the EMG collected during the baseline (robot-off) phase. The threshold was calculated as 20% of the maximum EMG entropy amplitude. This threshold was adapted for each repetition during the training (robot-on) phase. This strategy was used to encourage the user's effort throughout the entire rehabilitation process. This way, the device does not provide assistance if not needed and provides only as much as needed.

At the beginning of the session, baseline data were collected, and velocity and performance parameters were collected. The performance parameters were also calculated for each move, letter

A to letter B being one move, B to C another move, and so on, similar to the process proposed by Krebs *et al*. (28). The first performance parameter is the average deviation from the trajectory measured as follows:

$$P_1 = \frac{1}{N}\sum_{i=1}^{N} d_i \; where: d_i = \sqrt{(x - x_i)^2 + (y - y_i)^2}$$

where (x, y) is the target position and (x_i, y_i) is the handle position, and N the number of samples. Therefore, P_1 represents the average of the distance between the PHANTOM handle and the target along the trajectory. If a subject takes longer to start moving and "wobbles" around the shortest linear distance between the handle and the target, P_1 increases. On the other hand, a quick and linear movement from the handle position to the target yields a lower value of P_1. Figure 2 shows an example of the d_i measurements along a trajectory with the subject moving the handle from letter A to letter B.

Figure 2: Performance parameter P_1.

The second performance measure is the root-mean-square deviation along with the normal distance to the target axis measured as following:

$$P_2 = \sqrt{\frac{1}{N}\sum_{i=1}^{N} dn_i^2} \; where: dn_i = \frac{|(y_b - y_a)x_i - (x_b - x_a)y_i + x_b y_a - y_b x_a|}{\sqrt{(y_b - y_a)^2 + (x_b - x_a)^2}}$$

where dn_i is the normal distance to the target axis as defined above. The coordinates (x_a, y_a) represent the position of the letter of origin, (x_b, y_b) is the coordinates for the target letter, and (x_i, y_i) is the handle position. Therefore, P_2 represents the summation of the distance between the PHANTOM handle and the line from the previous target to the next target. In this equation, the reference is the smallest distance between the two targets. Hence, if the patient has high dexterity

and coordination, P_2 is small; otherwise, as shown in Figure 3, the P_2 increases. Figure 4.3 represents the subject moving the handle from letter A to letter B.

Figure 3: Performance parameter P_2.

Participants

Five chronic post-stroke patients were enrolled in this study. This sample size is consistent with many previous studies where robot-assisted therapy's performance was evaluated (21-25).

Table 1: Subject's information table.

Before the experiment, each subject was informed of the study requirements and was asked to provide written informed consent. Both sexes were included in this study. The stroke must have occurred at least six months ago. Participants had to be able to actively move their shoulder, elbow, and wrist, as determined by an occupational physiotherapist. Excluded were those who had: history of severe neurological injuries other than (spinal cord injury or stroke); severe concurrent medical diseases: infections, circulatory, heart or lung, pressure sores; problematic spasticity (e.g., Modified Ashworth ≥3); severely compromised arm function (Fugl-Myer score < 21 on the upper-extremity scale); heterotopic ossification; significant contractures; psychiatric or cognitive situations that may interfere with the proper operation of the device; cognitive impairments resulting in an inability to follow directions; poor skin integrity in areas in contact with the device; uncontrolled Autonomic Dysreflexia; and functional visual field or hemispherical neglect. These exclusion criteria were selected based on previous research studies of robot-assisted therapy in a clinical population with impaired arm (6,16,18,26).

The study protocol (REB 2019-073) was reviewed and approved by UNB Fredericton Research Ethics Board. The protocol was also reviewed and approved by the Horizon Health Network Research Ethics Board (case number 100273). All participants provided written informed consent after a full explanation of the research and the experiment.

Experimental procedures

The participant was seated in a height-adjustable chair with their arms in an initial position with the elbow at 90 degrees flexion on a tabletop with a monitor under the tabletop facing up. The PHANTOM device was positioned in front of them, as shown in Figure 4.

Figure 4: Diagram of the algorithm used during the training phase.

The table was a transparent plexiglass acrylic sheet on top of a monitor mounted to a metal structure. The monitor showed the letters, as shown in Figure 5. The patient was asked to hold the robotic arm's end effector and move until it touches the letters. They were able to feel when they reached the letter through a haptic force (touch effect) programmed in the robot. One letter was shown at a time.

Figure 5: The monitor projecting all the letters at once.

Prior to data collection, MAS and FMA scores were acquired. The patients were also asked to inform the activities they were involved in the previous weeks that involved any physical activity, using the ARM-A questionnaire.

The next step was to set up the EEG and EMG electrodes. The subject was asked to wear a cap where the EEG electrodes were placed, as shown in Figure 6. The EEG electrodes required gel between the sensor and scalp to reduce the impedance. This procedure usually took around 15 minutes. The EMG sensors were placed directly on the participant’s skin with a sensor adhesive interface. Nine EEG electrodes and six EMG electrodes were placed on the subject.

Figure 6: Subject wearing the EMG sensors and the cap for the EEG sensor.

The position of the 9 EEG electrodes is shown in Figure 7. The electrodes used in this protocol were the CF3, CF4, C3, C4, CP3, CP4, P3, P4, and Pz.

Figure 7: Position of the EEG sensors.

Six tests involving a planar 2 degree of freedom (DOF) reach task were performed: one for a baseline and five for the training. The data collection took around 45 minutes to one hour. In the first protocol, called baseline, which was used to acquire baseline characteristics, the subject was asked to reach the letters appearing in the monitor. The letters appeared in alphabetical order, one at a time, three times. First, only the first line of letters, A to E, shows up on the screen. Initially, we evaluated simple horizontal tasks with the elbow bent at this point. Next, the second line of letters, F-J shows up, again to evaluate horizontal tasks but increasing the elbow extension. Finally, the last line of letters again shows up to evaluate horizontal tasks and increase elbow extension. The letter positions can be seen in Figure 8.

Figure 8:Letters diagram.

After that, letters appeared in a sequence which the subject had to reach. For example, letter A shows first, then letter F, so the subject simulates a reaching forward task with the elbow half extended. Next, letter B appears, then letter H simulating lateral reaching with elbow half extended, and so on. The participant is given 5 seconds to reach the target without the assistance of the robot. During this baseline test, if they are unable to get to the target within 5 seconds, the target disappears, and the next target shows up on the screen.

The baseline phase was used to collect information such as ROM, velocity, force, and electromyography signal (EMG). No assistance was provided from the robot during the baseline phase.

For the following training protocols, the patient had to repeat the same movements as the baseline phase. However, this time, the letters appeared on the screen randomly. The letters appear 30 times for training tests one, two, and three, and 60 times for training tests four and five, with an interval between them of 5 seconds. The subjects had 60 seconds to rest between the tests. In this

part of the training, the robot-arm was assisting the participants when needed; if the patient could not reach the target, the robot-assisted, the patient in getting to the target. The robot was continuously evaluating the participant's EMG signal throughout the entire trajectory to achieve the target and only assists if the EMG signal is still detectable and there is no movement. The robot also applied some resistance to challenge the participant if both the velocity and the EMG were higher than the EMG and velocity threshold. The EMG signal threshold necessary for the robot to assist/resist increased based on the participant's improvement.

Data analysis

This study collected EEG, sEMG, and performance data in order to analyze the effectiveness of the novel AAN algorithm. The sEMG signal was used as an input for the control system and was also used to assess the training effects in conjunction with the performance parameters and EEG data. Internal validity of the system's responses was evaluated by using curve fitting methods to assess the relationship between the participant's FMA scale and performance metrics (average velocity, parameter P_1 and P_2), EMG entropy and EEG power density. Details of the analyses follow.

The performance parameters were first normalized by dividing the mean P1 and mean P2 by the assistance-resistance force (positive/negative force) provided by the robot during training.

To calculate the mean EMG entropy, we created an index based on the MAS summation, which gave us a normalized spasticity score from 1 to 10 and used to normalize the overall mean EMG entropy for every participant. This variable was called Mean Entropy, which represents the spasticity normalized mean entropy.

The EEG signal was first band-pass filtered from 1 to 30 Hz and visible artefacts were removed using an independent component analysis procedure to calculate the EEG spectra. Following this, the data were processed using a common average reference, and the data were divided into rest and active. The active and rest data were then divided into epochs of 2 seconds using a Hamming-window, and the power spectral density was calculated using the fast Fourier transform (FFT). The power spectral density was then averaged for each condition.

To answer research questions 1 and 2, EMG and EEG measurements were compared between the robot off (baseline) and on (training) conditions. To answer research questions 3

through 5, curve fitting was used to quantify the relationship between functional status (via the FMA score) and training outcomes measures: performance metrics, EMG, and EEG. Polynomials and rationales were used to find the simplest equation that best fit the experimental data. These analyses will provide internal validity whereby performance parameters, muscle and brain signals, are expected to vary with the user's functional status, thereby revealing the system's sensitivity.

Results

To demonstrate the movement task and its relative difficulty for the participants to perform, Figure 9 shows the hand horizontal trajectory for two participants: the highest functioning (FMA=65) and lowest functioning (FMA=36) during a task that required reaching a letter target and returning to the start letter.

Figure 9: a- Trajectory Y-X from the subject with FMA score of 65; b- Trajectory Y-X from the subject with FMA score of 36.

As can be seen in Figure 9, the higher functioning participant moved smoothly between targets with only moderate difficulty returning to the start point. In contrast, the lower functioning participant had difficulty reaching the target and often did not return to the origin before having to move to the next target.

This demonstrates that the population sample was appropriate for the study. Below we present the results of testing the algorithm's effect on the main outcomes measures and their relationships with (sensitivity to) functional status.

Effect of the aAAN algorithm

Research question 1 tested if EMG increases when using the aAAN algorithm in training compared to baseline (with robot off). The EMG entropy for each of the six muscles for the high and low functioning participants can be seen in Figure 10.

Figure 10: Entropy from 6 muscles -medium deltoid (MD); anterior deltoid (AD); posterior deltoid (PD); major pectoralis (MP); biceps (BI); triceps (TRI). (a) From a subject with an FMA score of 65 during baseline and training. (b) From a subject with an FMA score of 36 during baseline and training.

EMG entropy was combined across muscles and time for each participant in their baseline and training sessions and normalized to (divided by) spasticity index. These data are shown in Figure 11. The mean increase in normalized EMG entropy between baseline and training was statistically significant ($t=3.73$, $df=4$, $p=.02$), showing that slacking was always being avoided regardless of functional status.

Figure 11: Mean EMG entropy during baseline (robot off, blue) and training (robot on, orange) for participants in the trial. Top: Raw entropy values. Bottom: Entropy normalized to spasticity index.

Research question 2 was to test if EEG activity increases when using the aAAN algorithm during training relative to baseline. Brain activity maps using the EEG data can be seen in Figure 12 for baseline (robot off) and training (robot on).

Figure 12: EEG power density distribution for each subject during baseline and training.

Although there was no statistically significant change in EEG spectral density between baseline and training ($t=1.18$, $df=4$, $p=0.31$), the difference trended toward increased EEG activity.

Relationships to Functional Status

Research question 3 evaluated the relationship between functional status (FMA score) and normalized performance metrics P_1 and P_2. Based on the equation used to calculate the performance parameters P_1 and P_2, lower values mean better dexterity and coordination. However, when dividing this value by the assistance-resistance force, a higher P_{1norm} and P_{2norm} values represent better performance. This happens because the assistance-resistance force goes from -6 to +6, where a negative force represents robot resistance, and a positive represents assistance.

The results showed that performance parameter mean P_1 could be predicted from the clinical FMA score by following the formula from general model rational with coefficients (with 95% confidence bounds) and $R^2 = 0.9955$:

$$f(x) = (2.549 * x - 181.4)/x - 31.72$$

The fitted curve for the parameter FMA and mean P1 is shown in Figure 13. The shaded region shows P1norm is sensitive to functional status in the lower FMA score region.

Figure 13: Fitted curve for performance parameter FMA related to normalized P_{1norm}.The shaded region shows P_{1norm} is sensitive to functional status in the lower FMA score region.

Similarly, the performance parameter mean P_{2norm} could be predicted from the clinical FMA score by following the formula from a general model rational with coefficients (with 95% confidence bounds) $R^2 = 0.9996$:

$$f(x) = (9.078 * x - 708.6)/ x - 33.27$$

The fitted curve for the parameter FMA and mean P2 is shown in Figure 14. The shaded region shows P2norm is also sensitive to functional status in the lower FMA score region.

Figure 14: Fitted curve for performance parameter FMA related to normalized P_{2norm}. The shaded region shows P_{2norm} is sensitive to functional status in the lower FMA score region.

The average velocity achieved during training can also be predicted from the clinical FMA score by following the formula from a linear model polynomial with coefficients (with 95% confidence bounds) $R^2 = 0.9964$:

$$f(x) = (2.24e^{-05} * x^2 - 0.001908 * x + 0.08747)$$

The fitted curve for the parameter FMA and average velocity is shown in Figure 15. Conversely, the shaded region shows velocity is sensitive to functional status in the higher FMA score region.

Figure 15: Fitted curve for performance parameter FMA related to the average velocity. The shaded region shows velocity is sensitive to functional status in the higher FMA score region.

The results showed that the mean EMG entropy could be predicted from the clinical FMA score by following the formula from the linear model with coefficients (with 95% confidence bounds) $R^2 = 0.8073$:

$$f(x) = (1.54e^{-04} * x^2 - 0.01325 * x + 0.9867)$$

The fitted curve for normalized EMG entropy versus FMA is shown in Figure 16. Likewise, the shaded region shows EMG Mean Entropy is sensitive to functional status in the higher FMA score region

Figure 16: Fitted curve for clinical assessment FMA related to Mean Entropy. The shaded region shows EMG Mean Entropy is sensitive to functional status in the higher FMA score region.

The mean EEG signal was calculated for channels CF3, CF4, C3, C4, CP3, CP4, P3, P4, and PZ for the high beta wave range (16 - 24Hz), and the results showed that EEG activity could be predicted from the clinical assessment FMA by following the formula from linear model 3rd degree polynomial with coefficients (with 95% confidence bounds) $R^2 = 0.965636$:

$$f(x) = (3.157e^{-15} * x^2 - 2.757e^{-13} * x + 6.013e^{-12})$$

The fitted curve for the parameter FMA and EEG activity is shown in Figure 17. As above, the shaded region shows EEG spectral density is sensitive to functional status in the higher FMA score region.

Figure 17: Fitted curve representing the relationship between the EEG signal and the FMA scale. The shaded region shows EEG spectral density is sensitive to functional status in the higher FMA score region.

Discussion

This paper describes the development and validation of a new EMG-based adaptive AAN algorithm that adapts to user requirements in real-time based on performance and EMG entropy, providing assistance and resistance as needed to improve robot-assisted rehabilitation for the post-stroke population. To date, no study has done a comprehensive analysis to validate the sensitivity of an aAAN algorithm and method for delivering upper-extremity rehab training to patients with chronic hemiplegia post-stroke.

The algorithm developed in this study used an online adaptive control system based on physiological measures, specifically intending, to avoid slacking behavior and improve engagement during training. The robot was used to assist and challenge the patient during treatment, keeping them engaged throughout the entire training. To better understand the potential of this new method to impact people with stroke, we first compared EMG and EEG between the robot off and on states to test whether training with the aAAN algorithm increases peripheral and central activity, respectively, and; we evaluated how sensitive the performance and electrophysiological outcome measures were to the user's functional status.

Overall, the behavior of the system and how it challenged participants based on their functional status (as shown in Figure 4.6) was consistent with results presented by Krebs et al. (28) and Benitez (4). Although our sample size was small, based on these findings, we are confident

the post-stroke sample we recruited represented a sufficiently broad range to evaluate the behavior of the new aAAN algorithm.

Results of research questions 1 and 2 showed us that we achieved the aim of avoiding slacking by providing a challenge at all times, which can be seen in Figure 4.7 where the muscle activity increased during training (robot on) when compared to the baseline (robot off) even for the subject with a low score, showing that the slacking behavior is not happening even when the robot is assisting the subject as expected. This contradicts the results presented by Dipietro et al. (29), where the EMG signal was also used to trigger the robot, and their results showed that when the robot was on, the EMG amplitude reduced for all subjects. The authors explain this decrease in EMG as a validation that their robot was assisting the subject in completing the task, but it also indicates that slacking might occur. In contrast, our results showed that slacking never occurred (see Figure 4.8) when the robot was assisting, which was accomplished by the algorithm adding sufficient challenge when performance was good.

Another relevant finding was that higher brain activity was observed during training for some subjects (Figure 4.9), which is expected when more effort is required from the participant (13, 14, 17). Although there was only a small change for some subjects, resulting in a statistically insignificant difference, the trend was increasing. This represents that the participant had to do more work when the robot was on, which may infer that the robot's use increases the engagement needed from the subject, potentially improving neuroplasticity in the long term.

Research questions 3 through 5 showed there was a strong relationship between functional status and measurement outcomes, but the relationship was not a simple straight-line linear relationship; rather, it was always a higher-order equation that best fit the data, as seen in Figures 4.10 through 4.14. The curves' shapes were particularly revealing in terms of what might be expected as functional status improves with continued training.

Performance parameters P_{1norm} (Fig. 4.10) and P_{2norm} (Fig. 4.11) were more sensitive to change in participants with lower FMA scores, suggesting that these parameters may be more important to monitor subjects with more severe limitations at an earlier stage of motor recovery. Conversely, the results for velocity (Fig. 4.12), mean EMG entropy (Fig. 4.13), and EEG spectral density (Fig. 4.14) showed that these outcomes were more sensitive to change in participants with higher functional status.

Based on these findings, it may be hypothesized that participants with lower functional status may be expected to improve more in their performance measures before showing significant changes in muscle and brain activity during a longitudinal study of repeated training sessions. On the other hand, participants with higher functional status would have little performance improvement (already performing quite well). Still, they would show higher muscle and brain activity changes due to the increased challenge introduced by the aAAN algorithm for these patients. Future studies will be needed to verify if the novel control system can accelerate motor recovery over time.

Conclusion

This paper presented a new EMG-based adaptive AAN algorithm that was tested in five stroke subjects across a range of FMA scores from low UE sensory-motor function to high UE sensory-motor function during one session. A comprehensive analysis was performed to understand the algorithm's effectiveness regarding the brain, muscle activity, and performance improvement. Unlike other adaptive AAN algorithms, this new algorithm adapts in real time to the participant's needs based on their performance and EMG entropy, providing assistance and resistance as needed. The preliminary results were very promising; slacking was avoided for all participants during training with the aAAN controller. The system's sensitivity made sense from a motor learning perspective that the clinician can exploit to direct and monitor rehabilitation progress. Future studies with a larger sample size will be necessary to confirm the effectiveness of the new algorithm. Moreover, a complete treatment should be accomplished with weekly training sessions for a long period to understand the effects of the use of this new algorithm on a long-term basis.

Acknowledgements

Clinical staff, including physicians, and occupational therapists of the Stan Cassity Center for Rehabilitation and the Horizon's Dr. Everett Chalmers Regional Hospital; (IBME) Institute of Biomedical Engineering from the University of New Brunswick.

Authors' contributions

This study designed and tested an automated patient-cooperative system for promoting neuroplastic changes in cortical function by adapting the robot to provide assistance and resistance only as needed, based on the subject's muscles activity and performance parameters. To the author's knowledge, there are no published studies that have examined

if a relationship exists between the change in performance and changes in brain activity patterns during an upper-extremity training therapy that uses AAN control. The preliminary results show that this strategy is a more effective robotic-assisted therapy that can improves rehabilitation outcome. AA developed the aAAN system, tested on the patients, analyzed the results, is the major contributor in the writing manuscript. NB contributed in the development of the system, contributed in the analysis and in writing this paper. CM contributed in the contributed in the development of the system, contributed in the analysis and in writing this paper. All authors read and approved the final manuscript.

Funding

The studies were partially funded by the New Brunswick Innovation Foundation through a research assistantship initiative and by the Brazilian foundation Coordination for the Improvement of Higher Educational Personnel with the Brazilian Ministry of Education.

Availability of data and materials

The datasets used and/or analysed during the current study are available from the corresponding authors on reasonable request.

Ethics approval and consent to participate

The study protocol (REB 2019-073) was reviewed and approved by UNB Fredericton Research Ethics Board. The protocol was also reviewed and approved by the Horizon Health Network Research Ethics Board (case number 100273). All participants provided written informed consent after a full explanation of the research and the experiment.

Consent for publication

Not applicable

Competing interests

Not applicable

Authors details

[1]Ana Paula B. B. Arantes, [2]Nadja Bressan, and [1,3]Chris McGibbon; 1. Institute of Biomedical Engineering, University of New Brunswick; 2. Dept. Sustainable Engineering Design, University of Prince Edward Island; 3. Faculty of Kinesiology, University of New Brunswick

References

1. J. Mackay, G. A. Mensah, S. Mendis, and K. Greenlund, “The atlas of heart disease and stroke,” 2004.
2. J. C. Perry et al., “Design of a Spring-Assisted Exoskeleton Module for Wrist and Hand Rehabilitation,” IEEE Access, pp. 594–597, 2016.
3. D. J. Reinkensmeyer, J. L. Emken, and S. C. Cramer, “Robotics, motor learning, and neurologic recovery.,” Annu. Rev. Biomed. Eng., vol. 6, pp. 497–525, 2004.
4. L. M. Vaca Benitez, M. Tabie, N. Will, S. Schmidt, M. Jordan, and E. A. Kirchner, “Exoskeleton technology in rehabilitation: Towards an EMG-based orthosis system for upper limb neuromotor rehabilitation,” J. Robot., vol. 2013, 2013.
5. L. Y. Joo et al., “A feasibility study using interactive commercial off-the-shelf computer gaming in upper limb rehabilitation in patients after stroke,” J. Rehabil. Med., vol. 42, no. 5, pp. 437–441, 2010.

6. S. Ates, I. Mora-Moreno, M. Wessels, and A. H. A. Stienen, “Combined active wrist and hand orthosis for home use: Lessons learned,” in 2015 IEEE International Conference on Rehabilitation Robotics (ICORR), 2015, vol. 2015-Septe, pp. 398–403.
7. F. Vanoglio et al., “Feasibility and efficacy of a robotic device for hand rehabilitation in hemiplegic stroke patients: A randomized pilot-controlled study.,” Clin. Rehabil., 2016.
8. U. Jeong, H. In, H. Lee, B. B. Kang, and K. J. Cho, “Investigation on the control strategy of soft wearable robotic hand with slack enabling tendon actuator,” Proc. - IEEE Int. Conf. Robot. Autom., vol. 2015-June, no. June, pp. 5004–5009, 2015.
9. L. Marchal-Crespo and D. J. Reinkensmeyer, “Review of control strategies for robotic movement training after neurologic injury,” J. Neuroeng. Rehabil., vol. 6, no. 1, p. 20, 2009.
10. T. Proietti and V. Crocher, “Upper-Limb Robotic Exoskeletons for Neurorehabilitation: A Review on Control Strategies,” vol. 9, pp. 4–14, 2016.
11. L. L. Cai et al., “Implications of Assist-As-Needed Robotic Step Training after a Complete Spinal Cord Injury on Intrinsic Strategies of Motor Learning,” J. Neurosci., vol. 26, no. 41, pp. 10564–10568, 2006.
12. F. Resquín et al., “Hybrid robotic systems for upper limb rehabilitation after stroke: A review,” Med. Eng. Phys., vol. 0, pp. 1–10, 2016.
13. J. D. Schaechter, “Motor rehabilitation and brain plasticity after hemiparetic stroke,” Prog. Neurobiol., vol. 73, no. 1, pp. 61–72, 2004.
14. F. Buma, G. Kwakkel, and N. Ramsey, “Understanding upper limb recovery after stroke,” Restor. Neurol. Neurosci., vol. 31, no. 6, pp. 707–722, 2013.
15. C. D. Takahashi, R. A. Scheidt, and D. J. Reinkensmeyer, “Impedance control and internal model formation when reaching in a randomly varying dynamical environment.,” J. Neurophysiol., vol. 86, no. 2, pp. 1047–1051, 2001.
16. K. Y. Tong et al., “An intention driven hand functions task training robotic system,” in 2010 Annual International Conference of the IEEE Engineering in Medicine and Biology, 2010, pp. 3406–3409.
17. C. J. Winstein and D. B. Kay, “Translating the science into practice: shaping rehabilitation practice to enhance recovery after brain damage,” in Progress in Brain Research, 1st ed., vol. 218, Elsevier B.V., 2015, pp. 331–360.
18. F. Amirabdollahian et al., “Design, development and deployment of a hand/wrist exoskeleton for home-based rehabilitation after stroke - SCRIPT project,” Robotica, vol. 32, no. 08, pp. 1331–1346, 2014.
19. M. Casadio et al., “Robot therapy of the upper limb in stroke patients: Preliminary experiences for the principle-based use of this technology,” Funct. Neurol., vol. 24, no. 4, pp. 195–202, 2009.
20. B. A. Murphy, “High Intensity Exercise may be Needed to Change Levels ofcc Biomarkers Related to Neuroplasticity,” *Neuroscience*, vol. 437, pp. 240–241, 2020.
21. V. W. Oguntosin and E. Engineering, “Development of Soft Modular Robotics,” University of Reading, 2017.
22. L. Guenan, “Development and clinical feasibility of a novel pediatric arm rehabilitation robot,” ETH Zurich, 2014.
23. B. B. Kang, H. Lee, H. In, U. Jeong, J. Chung, and K. Cho, “Development of a Polymer-Based Tendon-Driven Wearable Robotic Hand,” pp. 3750–3755, 2016.
24. O. F. Salford, D. O. F. Philosophy, and A. Abdul-rahman, “Design and implementation of a control system for powered reciprocating gait orthosis school of acoustics and electronic engineering,” Univ. Salford, no. November, p. 308, 2000.
25. L. Meng, “Applied to rehabilitation in spinal the runbot: engineering control cord injury patients,” University of Glasgow, 2015.
26. R. Song, K.-Y. Tong, X. Hu, and W. Zhou, “Myoelectrically controlled wrist robot for stroke rehabilitation,” J. Neuroeng. Rehabil., vol. 10, no. 1, p. 1, 2013.
27. X. Zhang and P. Zhou, “Sample entropy analysis of surface EMG for improved muscle activity onset detection against spurious background spikes,” J. Electromyogr. Kinesiol., vol. 22, no. 6, pp. 901–907, 2012.

28. H. I. Krebs et al., “Rehabilitation robotics: Performance-based progressive robot-assisted therapy,” Auton. Robots, vol. 15, no. 1, pp. 7–20, 2003.
29. L. Dipietro, M. Ferraro, J. J. Palazzolo, H. I. Krebs, B. T. Volpe, and N. Hogan,“Customized Interactive Robotic Treatment for Stroke: EMG-Triggered Therapy,” *IEEE Trans Neural Syst Rehabil Eng.*, vol. 13, no. 3, pp. 325–334, 2005.

Figures

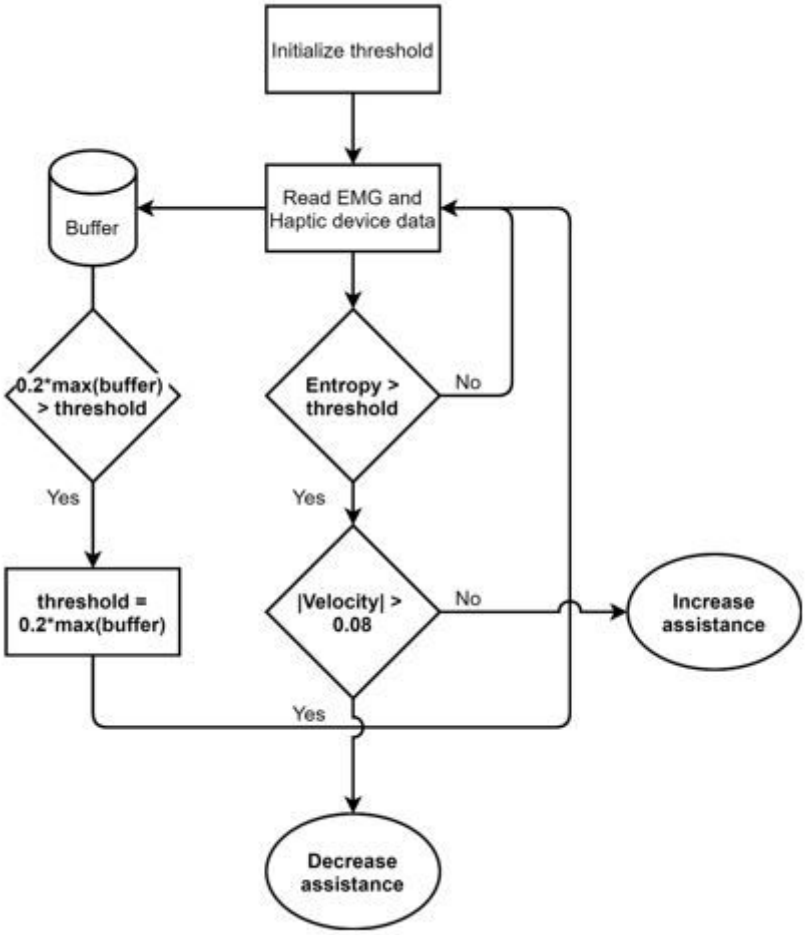

Figure 1

Patient-cooperative non-slacking system

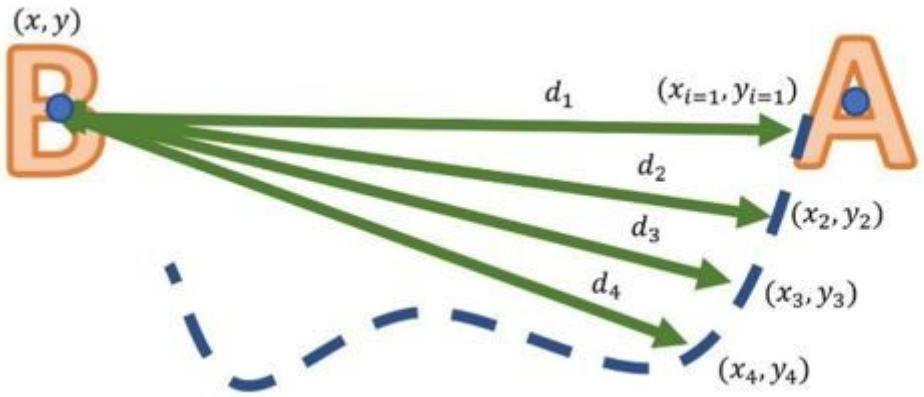

Figure 2

Performance parameter P1

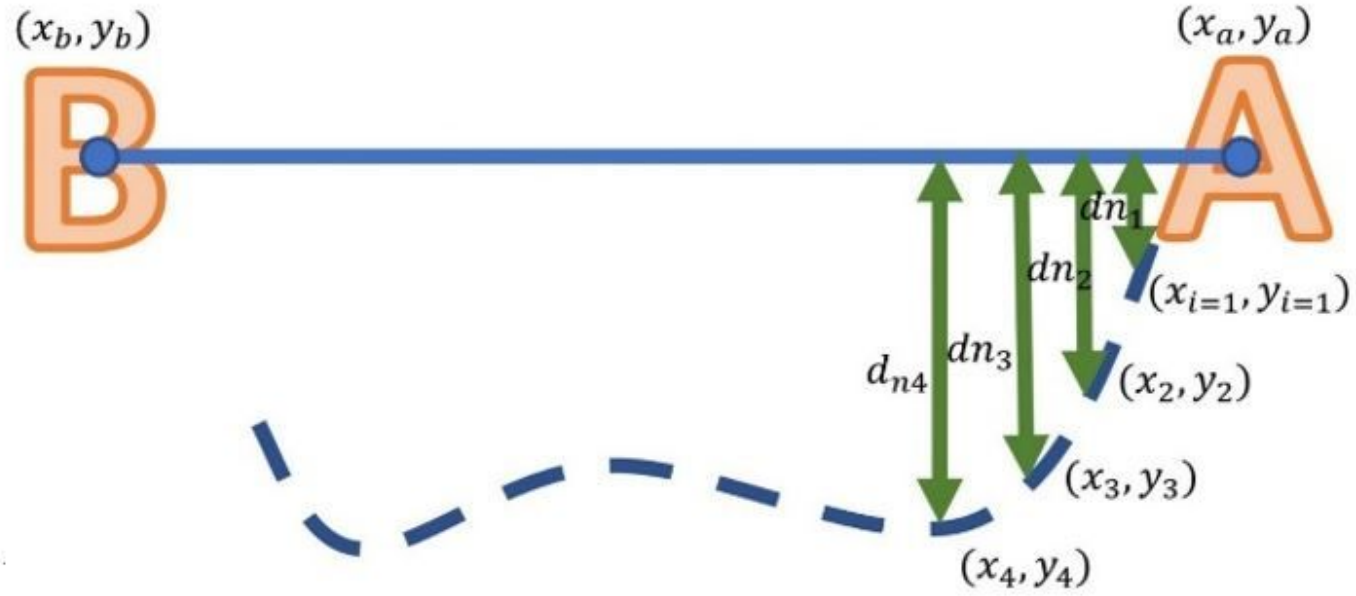

Figure 3

Performance parameter P2

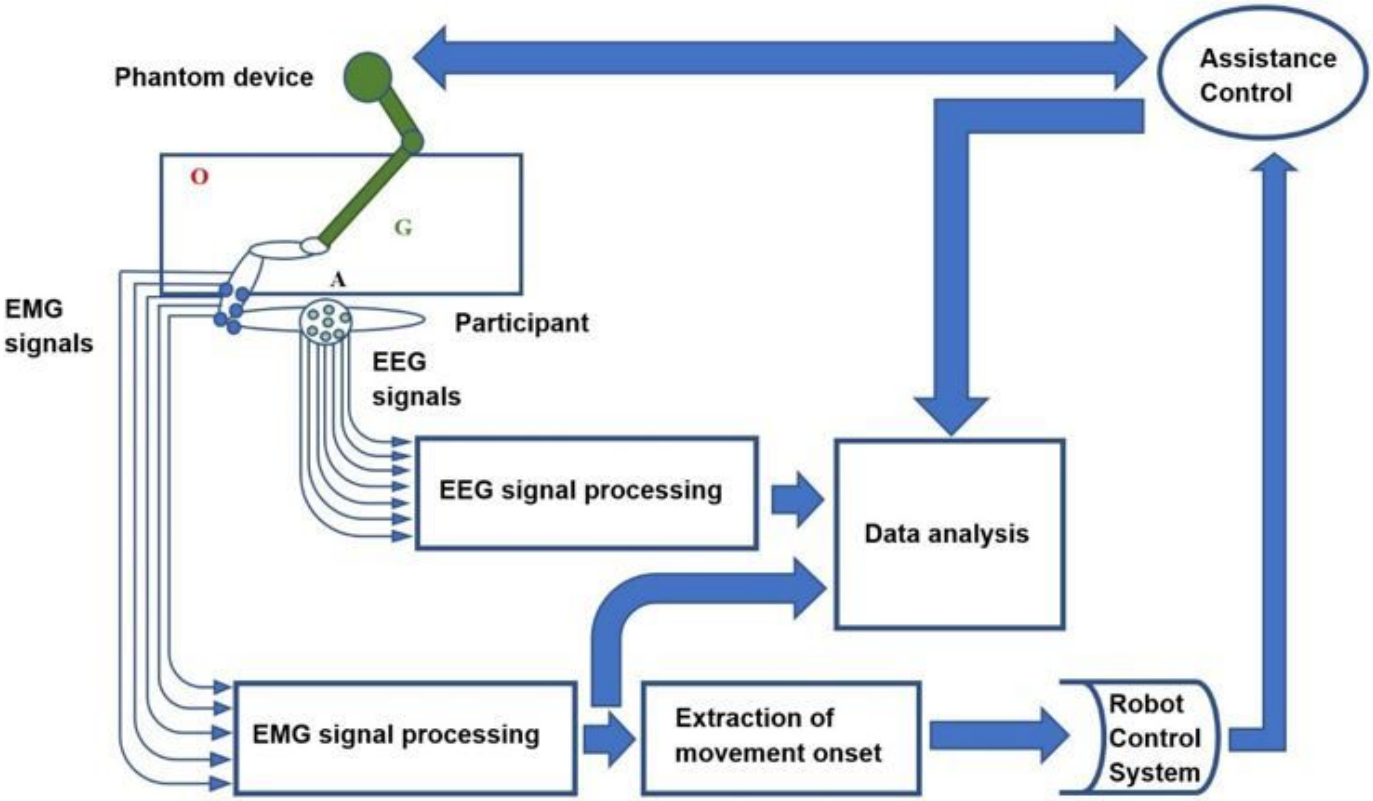

Figure 4

Diagram of the algorithm used during the training phase.

Figure 5

The monitor projecting all the letters at once.

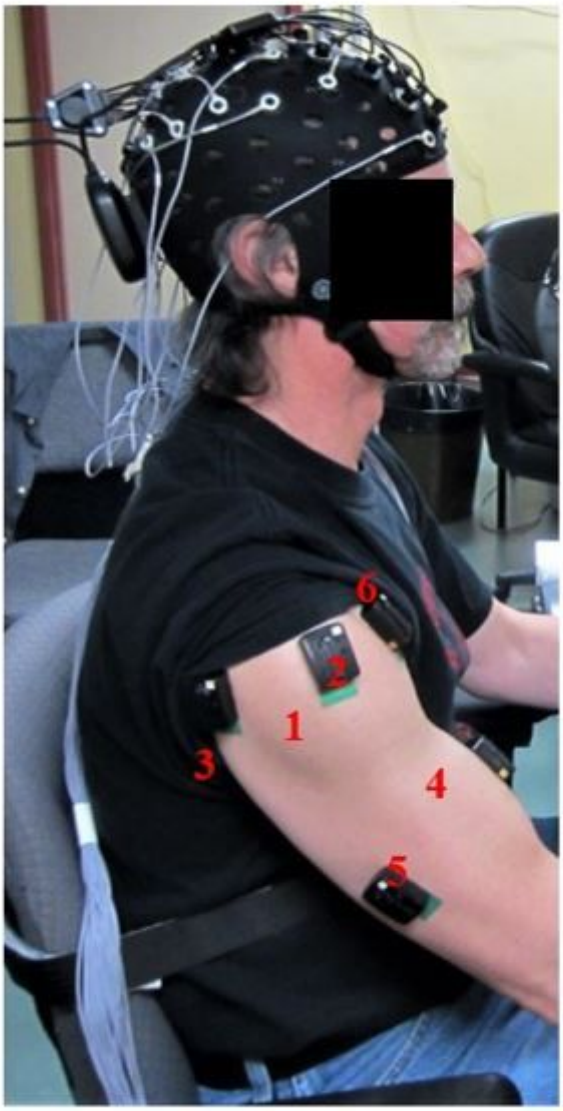

Figure 6

Subject wearing the EMG sensors and the cap for the EEG sensor.

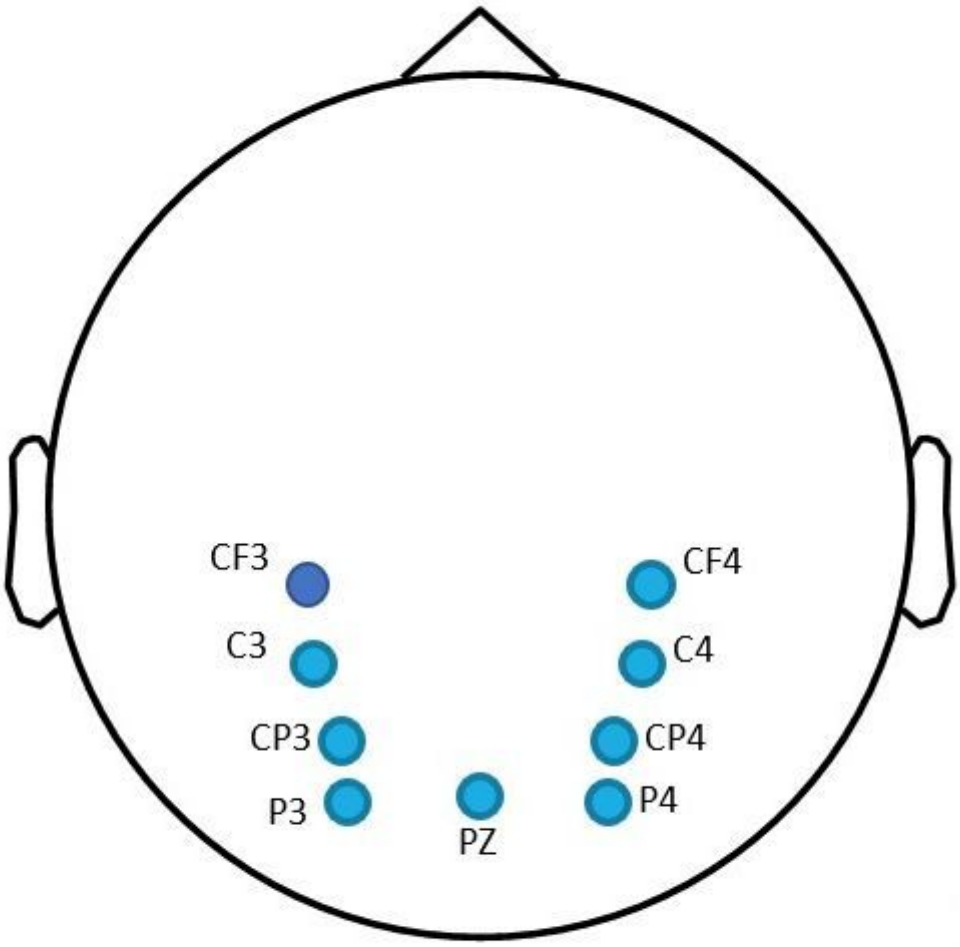

Figure 7

Position of the EEG sensors.

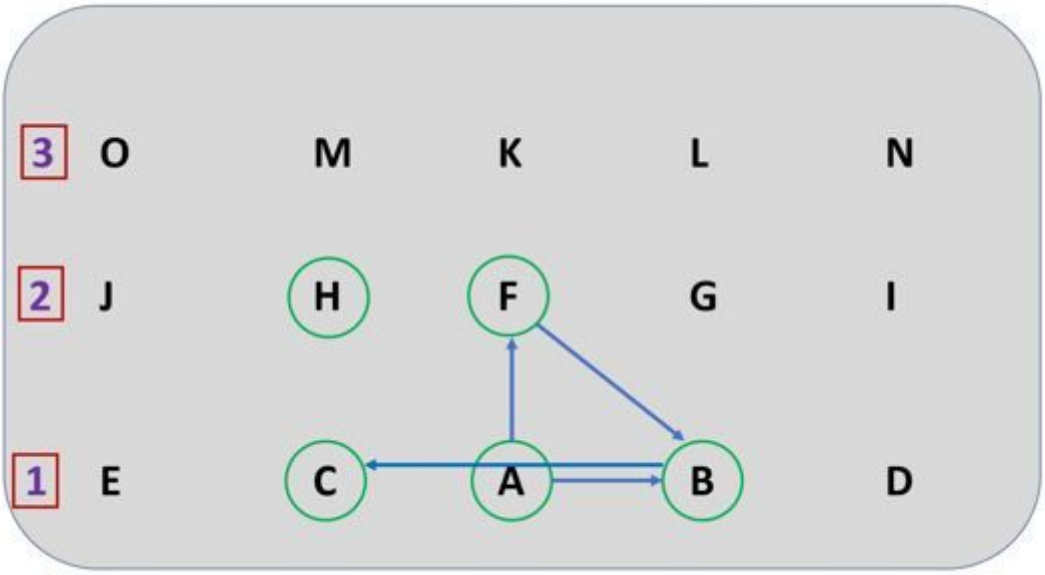

Figure 8

Letters diagram.

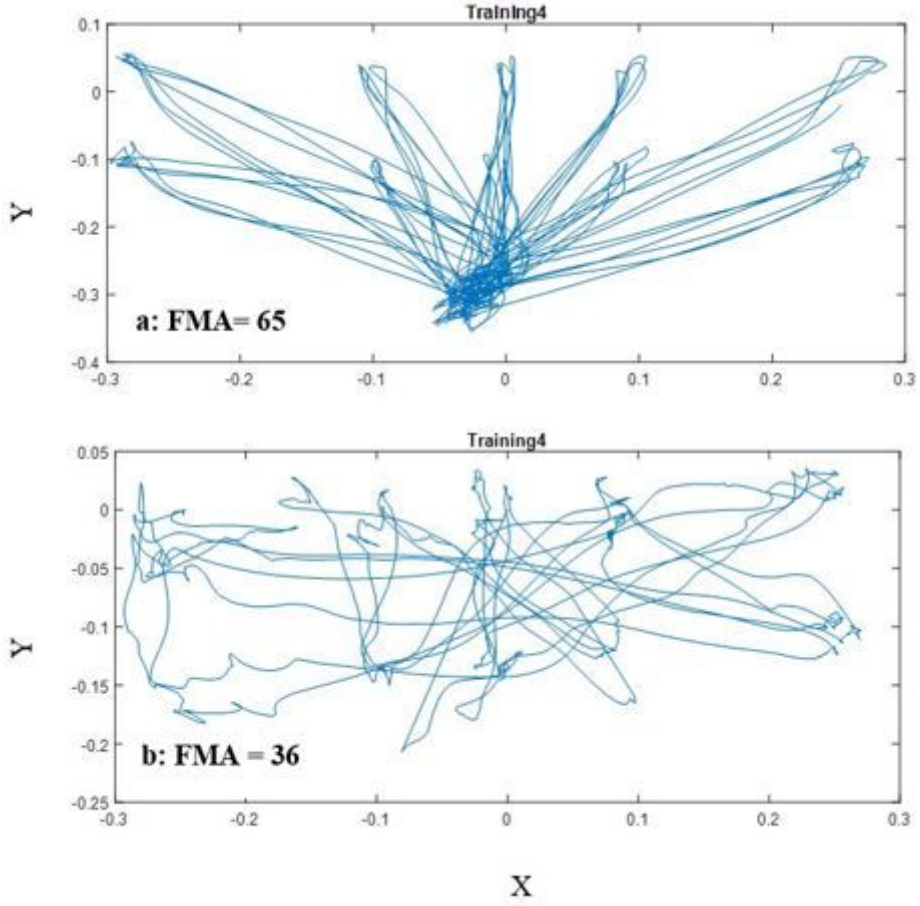

Figure 9

a- Trajectory Y-X from the subject with FMA score of 65; b- Trajectory Y-X from the subject with FMA score of 36.

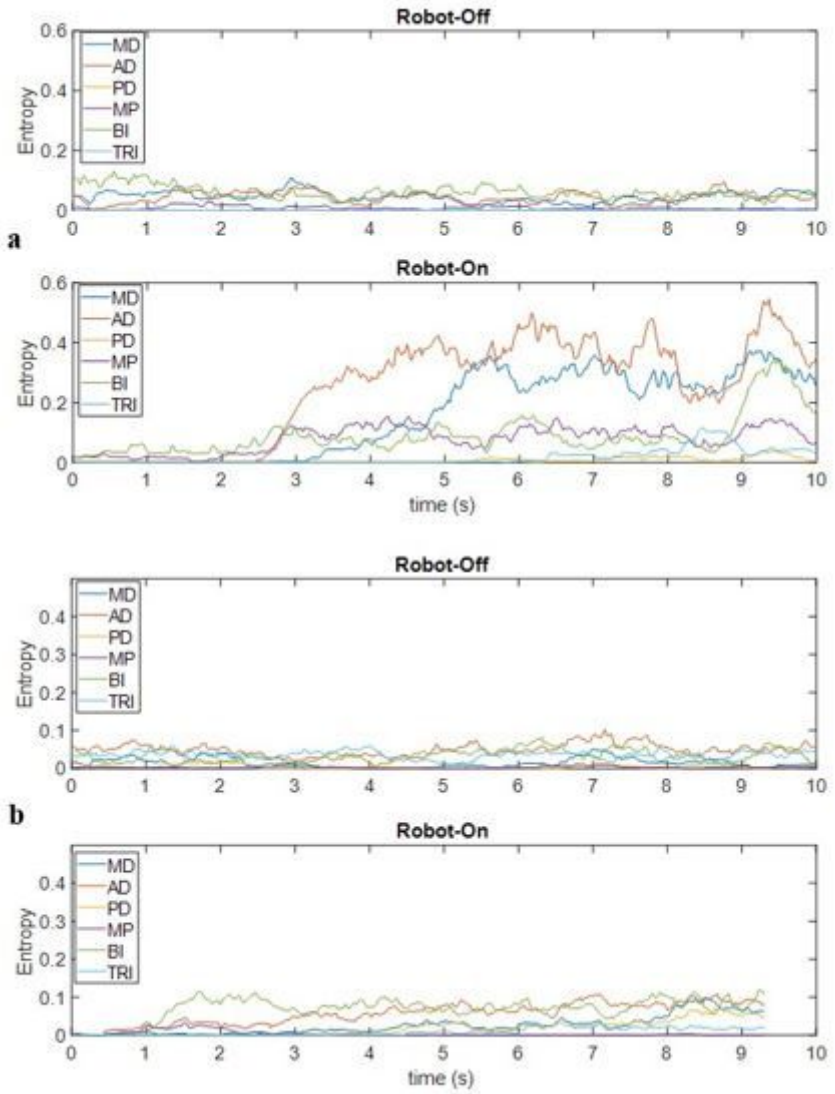

Figure 10

Entropy from 6 muscles -medium deltoid (MD); anterior deltoid (AD); posterior deltoid (PD); major pectoralis (MP); biceps (BI); triceps (TRI). (a) From a subject with an FMA score of 65 during baseline and training. (b) From a subject with an FMA score of 36 during baseline and training.

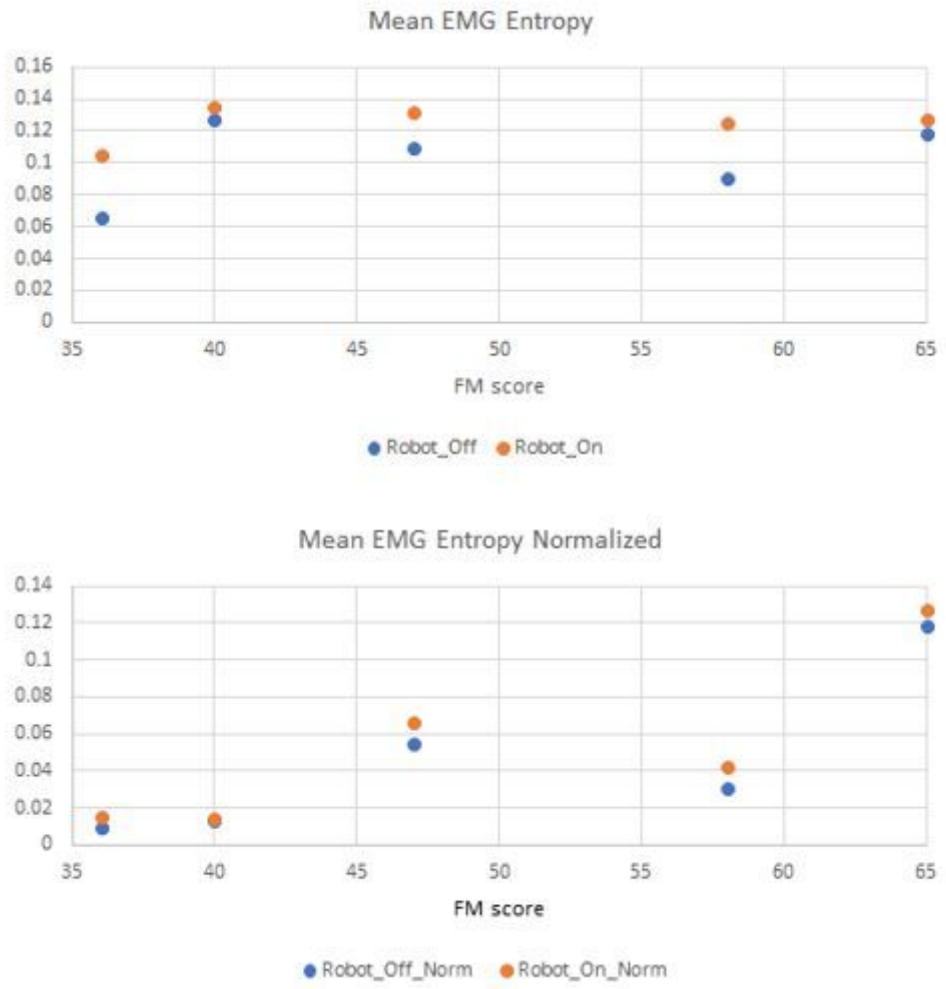

Figure 11

Mean EMG entropy during baseline (robot off, blue) and training (robot on, orange) for participants in the trial. Top: Raw entropy values. Bottom: Entropy normalized to spasticity index.

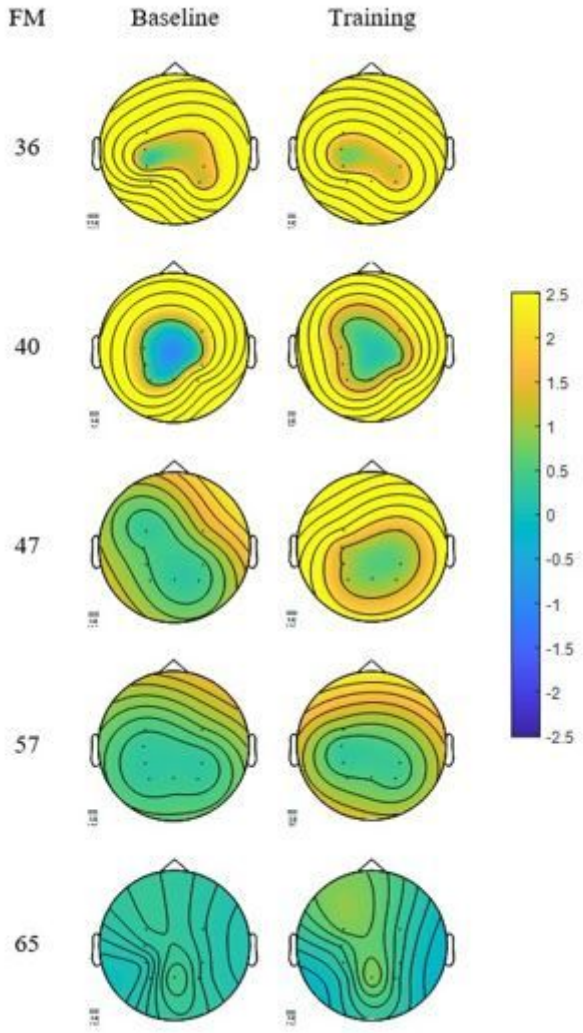

Figure 12

EEG power density distribution for each subject during baseline and training. Although there was no statistically significant change in EEG spectral density between baseline and training (t=1.18, df=4, p=0.31), the difference trended toward increased EEG activity.

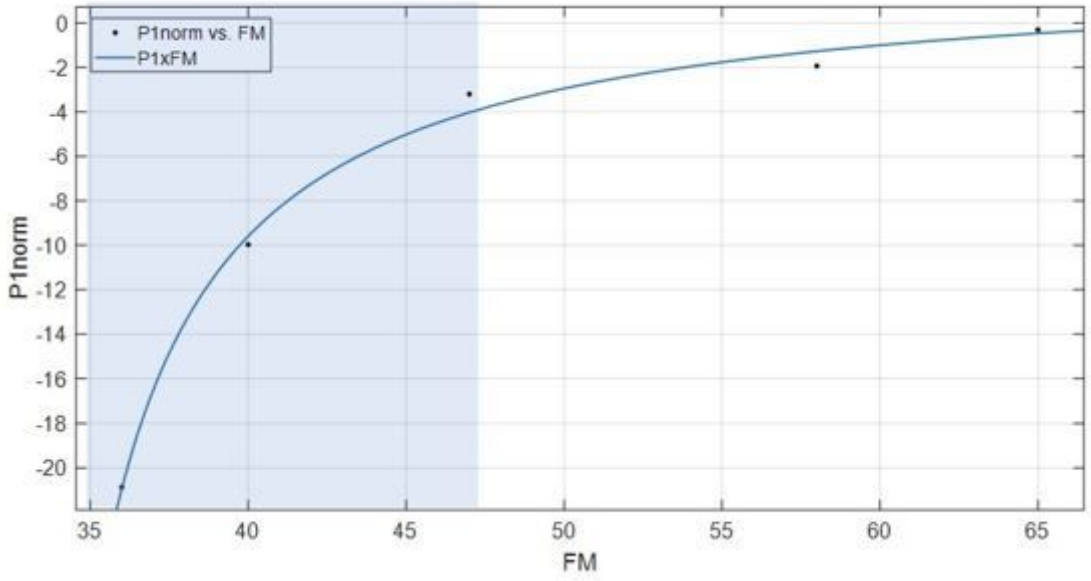

Figure 13

Fitted curve for performance parameter FMA related to normalized P1norm.The shaded region shows P1norm is sensitive to functional status in the lower FMA score region.

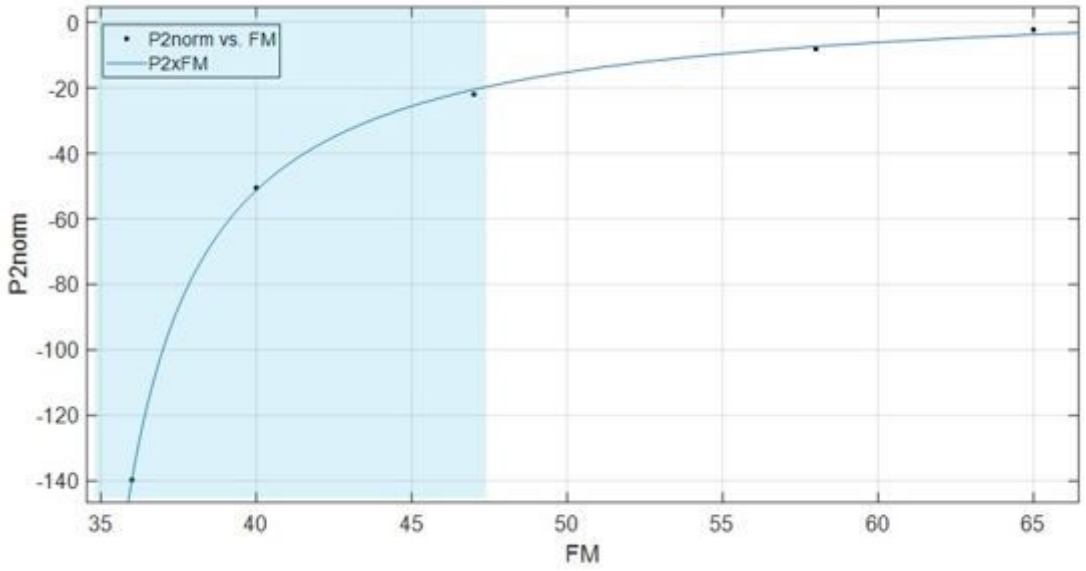

Figure 14

Fitted curve for performance parameter FMA related to normalized P2norm. The shaded region shows P2norm is sensitive to functional status in the lower FMA score region.

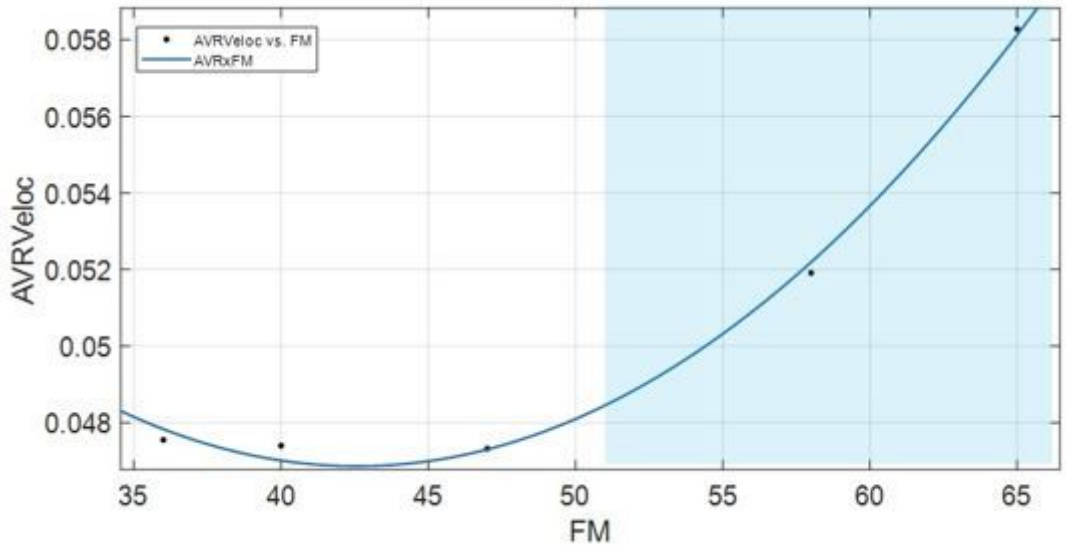

Figure 15

Fitted curve for performance parameter FMA related to the average velocity. The shaded region shows velocity is sensitive to functional status in the higher FMA score region.

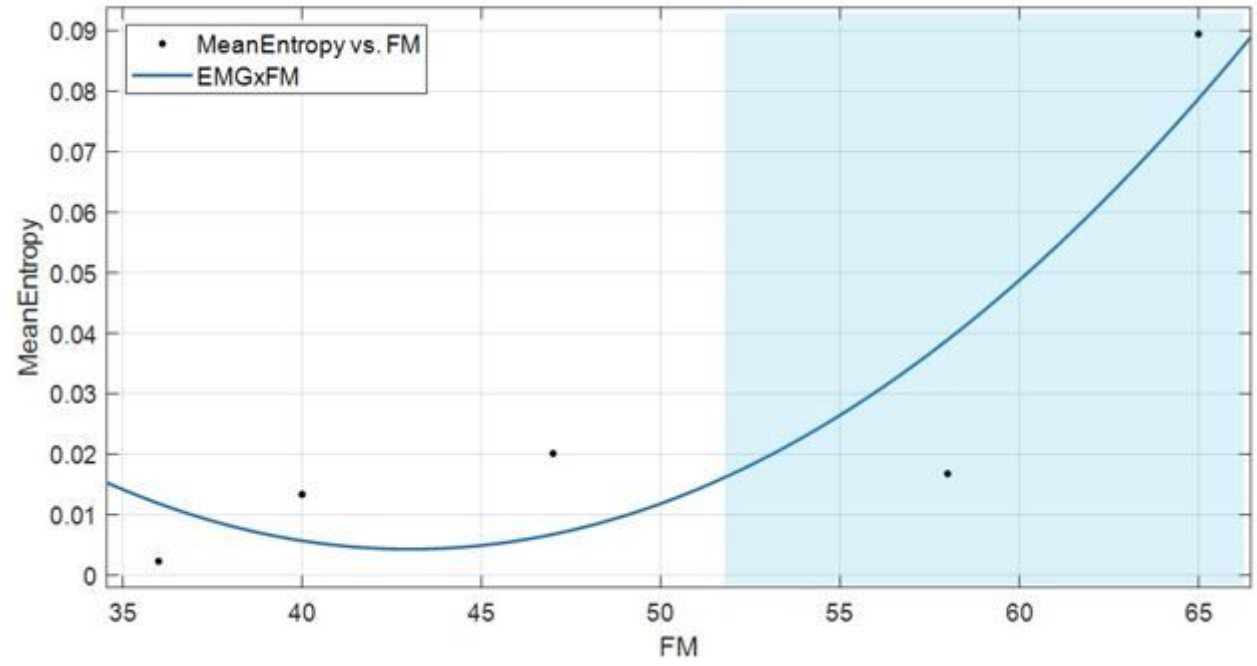

Figure 16

Fitted curve for clinical assessment FMA related to Mean Entropy. The shaded region shows EMG Mean Entropy is sensitive to functional status in the higher FMA score region.

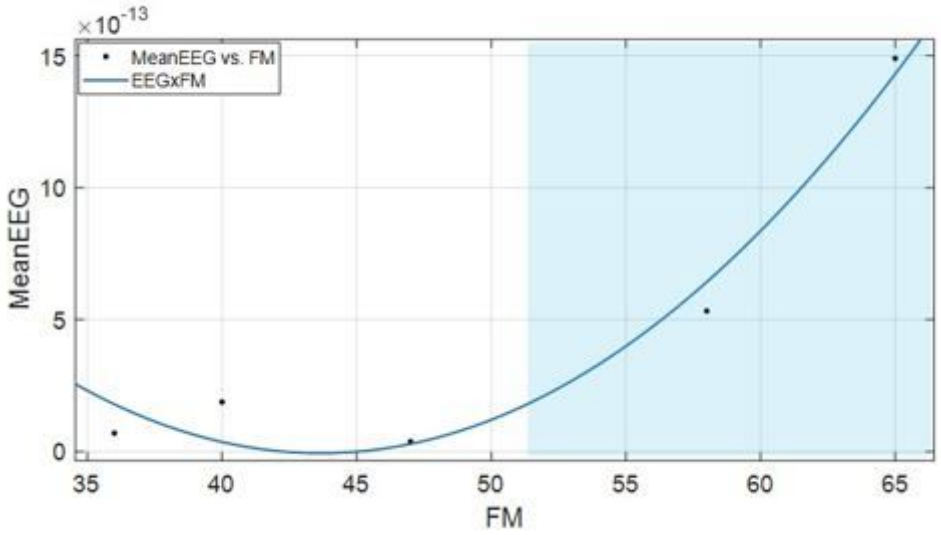

Figure 17

Fitted curve representing the relationship between the EEG signal and the FMA scale. The shaded region shows EEG spectral density is sensitive to functional status in the higher FMA score region.

Supplementary Files

This is a list of supplementary files associated with this preprint. Click to download.

- Table1.docx